PNAS
www.pnas.org

Supplementary Information for

Superconductivity found in Meteorites

James Wampler[a,b,1], Mark Thiemens[c,1], Shaobo Cheng[d], Yimei Zhu[d], Ivan K. Schuller[a,b,1]

[a]Department of Physics, University of California San Diego, La Jolla, CA 92093; [b]Center for Advanced Nanoscience, University of California San Diego, La Jolla, CA 92093; [c]Department of Chemistry and Biochemistry, University of California San Diego, La Jolla, CA 92093; [d]Condensed Matter Physics and Materials Science, Brookhaven National Laboratory, Upton, NY 11973

[1]Correspondance to: James Wampler, Mark Thiemens, Ivan K. Schuller

Email: jamespwampler@gmail.com, mthiemens@ucsd.edu, ischuller@ucsd.edu

This PDF file includes:

Supplementary text
Figures S1 to S4
Tables S1 to S6

Methods

Meteorite Selection Criteria. A diverse population of meteorites was measured (Table S3). Among chondrites, a range of chemical groups and petrologic types were measured. Among nonchondrites, primitive achondrites (including GRA 95205, a ureilite), magmatic achondrites (a eucrite, a diogenite and an aubrite) and two different irons (including Mundrabilla) were measured. In previous studies, we have also studied micrometeorites (1), martian meteorites and lunar rocks. Initially, meteorites with extreme formation conditions in their history were selected to measure (including both Mundrabilla and GRA 95205), although others were later added to represent other classes of meteorites. While no meteorite is fully representative of the range of interesting chemical phases within any given class of meteorites, this set of meteorites provided a good representative sample that spans the classes of meteorites (2). The piece of Mundrabilla from which all samples were obtained (inset of Fig. 1a) was obtained from the Field Museum of Chicago where it was cut but not otherwise processed (it was not polished, there was not a fusion crust on it, etc.). The pieces of GRA 95205 were obtained from Antarctic meteorite collection, curated at Johns Space Center and were not processed at that location.

MFMMS. During sample handling, extreme care is taken to ensure no outside contaminants are introduced. All work areas were layered with cleanroom wipes before sample processing was performed with clean tweezers and scalpels. Parent samples were obtained by scraping at the meteorite with stainless steel (i.e. non-superconducting) scalpels to dislodge metallic and

www.pnas.org/cgi/doi/10.1073/pnas.1918056117

nonmetallic fragments. Subsamples were obtained by sorting grains of the parent sample visually using an optical microscope.
Powder samples were inserted into quartz tubes for use in MFMMS. The quartz tubes were then flushed with helium and sealed. MFMMS measurements were performed with a variable DC Field, H_{DC}, and an AC Field, H_{AC}, of 15 Oe, applied parallel to the microwave magnetic field, as described previously (3). Measurements with sequences of DC fields applied (Fig. 1, 3) are applied in strictly increasing sequences (4).

VSM. Samples were measured in the Quantum Design PPMS Dynacool VSM option. Each sample that was measured in the VSM had previously been screened in MFMMS. In order to recover the powder from a MFMMS tube, the tube was broken and the powder was scraped out of the end of the tube in a clean environment. The resultant sample was then inserted into the VSM .
ZFC measurements of samples were performed by cooling without any applied magnetic field and then applying a field before measurement (4). FC measurements were performed at the same fields by applying a magnetic field and then measuring while heating. At 5 Oe and 10 Oe (Fig. 2c), five separate averages at each temperature point were taken consecutively, to account for the increased noise at these fields. For clarity, data in the images was offset from Fig. S2. In VSM measurements of sample MUND-2 (Fig. 2d), data was collected while temperature was sweeping – made possible by the increased signal in that sample.
VSM measurements were performed on samples from Mundrabilla due to the strength of the superconducting response in MFMMS and the larger number of superconducting samples found.

Sample Volume Measurements. VSM measurements give the magnetic moment of a sample. To calculate the average magnetization within a sample, it was necessary to determine the sample volume, which was difficult to do precisely. The two easiest methods that might be used were measuring volume by liquid displacement, and measuring the mass and converting to volume using a known density. The sample volumes were too small for most liquid displacement techniques, with sample volumes below 1 mm^2 (1 microliter displacement). And the density could not be easily determined: not only are these samples natural materials, but the methods described in this paper select out specific samples from the larger bulk, adding a strong selection bias.
Previous studies on micrometeorites have attempted to estimate volumes of samples with similar size scales as the grains measured in this paper by making inferences from 2D images. One study estimated volumes of approximately spherical samples by taking 2D images and assuming equal semiminor axes (5). Other studies estimate volume by imaging samples, outlining them, and then using a configuration with a low depth of focus to measure height (6, 7). However, the grains studied in this work are not approximately spherical (Fig. S3) and the height of the particles is insufficiently regular for the latter method. In order to come up with a volume estimate, we combined these two approaches, outlining the samples, and measuring a property termed the "local thickness" of each pixel in each grain to calculate an average in-plane thickness.
In order to determine the volume of the samples, the samples were imaged with an optical microscope and camera (4). ImageJ software (8) was used to outline and calculate the area of the samples (Fig. S4a, S4b). Using this outline, the local thickness was calculated (9) (Fig. S4c). Local thickness is defined as the diameter of the largest circle that could fit within the sample at each point. The out of plane thickness of the sample can then be roughly estimated by calculating the average local thickness. Note that this is not a direct measurement of the out of plane thickness, but simply an estimate based on the assumption that these samples are either approximately regular or approximately randomly oriented.
To quantify the error contribution of that assumption, multiple measurements were taken of very irregular grains from sample MUND-2, subsample A. These grains were placed inside a quartz tube and pictures were taken while the tube was rotated. The variance of this measurement gave an upper bound on this contribution to uncertainty, of 29.88% of a given sample's volume. The total error for a given volume estimate is calculated from that contribution, an approximate error of 0.05 mm^2 from outlining the samples, and the standard deviation in the local thickness for a

particular volume estimate. Using this method, the volume and uncertainty of samples could be estimated (Table S4).

Divide and Conquer. The Divide and Conquer process involved dividing samples into subsamples, in order to determine what grains within a sample contained superconductivity. In order to do this, samples were examined with an optical microscope and completely separated based on their visual morphology (a subjective assessment based on the appearance of individual grains) into different subsamples. This initial step was qualitative and the success or failure of it was determined by subsequent measurements. To do this, the subsamples were individually measured in MFMMS to determine which subsamples produced a superconducting response and how strong that response was (4). If some of the subsamples were not superconducting, they could be analyzed and compared with the superconducting ones, to determine what the superconducting phase was.

Scanning Electron Microscopy (SEM) EDX. Individual grains were selected from the subsamples resulting from the divide and conquer process and placed on carbon tape. These grains were then measured in an FEI Quanta 250 SEM using the EDX option (4). Multiple locations were measured in order to ensure that the surface was sufficiently homogenous. By examining the difference between superconducting and non-superconducting grains, it was possible to determine what elements were unique to the superconducting grains. By comparing these elements to the chemical makeup of known superconductors with critical temperatures near those measured in MFMMS, it was possible to determine the likely superconducting compound.

Superconducting Materials Database (SuperCon). In order to support the previous determination, the SEM-EDX data (Tables S5 and S6) was analyzed using information from the SuperCon database (10). An algorithm was written that compared each superconducting entry in SuperCon with T_c between 5 K and 8 K at ambient pressure to each set of EDX data (Fig. 4). These superconducting entries were sorted by the maximum possible volume percentage the phase could have within a given sample, assuming the EDX data was characteristic of the bulk of the sample (4). This data was sorted by this maximum volume percentage (Table S1). Specifically, the code performed the following steps on each EDX dataset:

1. Reads in all information from SuperCon and EDX dataset
2. EDX reports concentrations in mass percentage of the whole sample.
3. Compares each compound in SuperCon to the EDX dataset:
    a. Determine the total molecular mass of the compound
    b. For each element calculate $Mm_e/a_e n_e$, where M is the total molecular mass of the compound, m_e is the mass fraction of the element in the EDX dataset, a_e is the atomic mass of the element and n_e is the number of the element in the chemical formula of the compound.
        i. This gives the total possible weight fraction of the superconducting compound within the sample, based only one how much of that one element is available.
    c. Determine this number for each element in superconducting compound.
    d. The lowest of these numbers is total possible weight fraction of the superconducting compound within the sample.
    e. Convert weight fraction to weight percent
    f. Note that carbon and oxygen are ignored for these calculation due to the carbon tape background and potentially oxidized surface (which would not necessarily be representative of the interior).
4. Removes all superconducting compounds with T_c below 5 K or above 8 K or compounds of only carbon and oxygen.
5. Sorts the remaining superconducting compounds by the aforementioned possible weight percent

Compounds that were superconducting only under pressure were removed manually after the code ran. The code is available from the corresponding author upon reasonable request.

Transmission Electron Microscopy. Due to the large number of superconducting samples available, TEM measurements were performed on samples from the Mundrabilla meteorite (4). The samples were made by standard lift-out method by an FEI Helios dual beam system. The samples were further trimmed at low voltage mode to remove the surface amorphous layers. Elemental mappings were conducted on a high-resolution analytical transmission electron microscope (TEM, FEI Talos F200X) operating at 200 kV. The elemental mappings were acquired with a four-quadrant 0.9 sr energy dispersive X-ray spectrometer (Super EDX).

References

1. S. Guénon, *et al.*, Search for superconductivity in micrometeorites. *Sci. Rep.* **4**, 7333 (2014).
2. H. Y. J. McSween, G. R. Huss, *Cosmochemistry* (University Press, 2010).
3. J. G. Ramírez, A. C. Basaran, J. de la Venta, J. Pereiro, I. K. Schuller, Magnetic field modulated microwave spectroscopy across phase transitions and the search for new superconductors. *Reports Prog. Phys.* **77**, 093902 (2014).
4. J. Wampler, M. Thiemens, S. Cheng, Y. Zhu, I. K. Schuller, Data from: Superconductivity Found in Meteorites. UC San Diego Library Digital Collections. Available at https://doi.org/10.6075/J0KW5DDX. Deposited 31 January, 2020
5. C. Suavet, *et al.*, Magnetic properties of micrometeorites. *J. Geophys. Res. Solid Earth* **114**, 1–15 (2009).
6. G. J. Flynn, S. R. Sutton, Cosmic Dust Particle Densities: Evidence for Two Populations of Stony Micrometeorites. *Proc. Lunar Planet. Sci.* **21**, 541–547 (1991).
7. S. G. Love, D. J. Joswiak, D. E. Brownlee, Densities of Stratospheric Micrometeorites. *Icarus* **111**, 227–236 (1994).
8. C. A. Schneider, W. S. Rasband, K. W. Eliceiri, NIH Image to ImageJ: 25 years of image analysis. *Nat. Methods* **9**, 671–675 (2012).
9. R. Dougherty, K.-H. Kunzelmann, Computing Local Thickness of 3D Structures with ImageJ. *Microsc. Microanal.* **13**, 1678–1679 (2008).
10. , Superconducting Material Database (SuperCon). *Natl. Inst. Mater. Sci.* (2011).

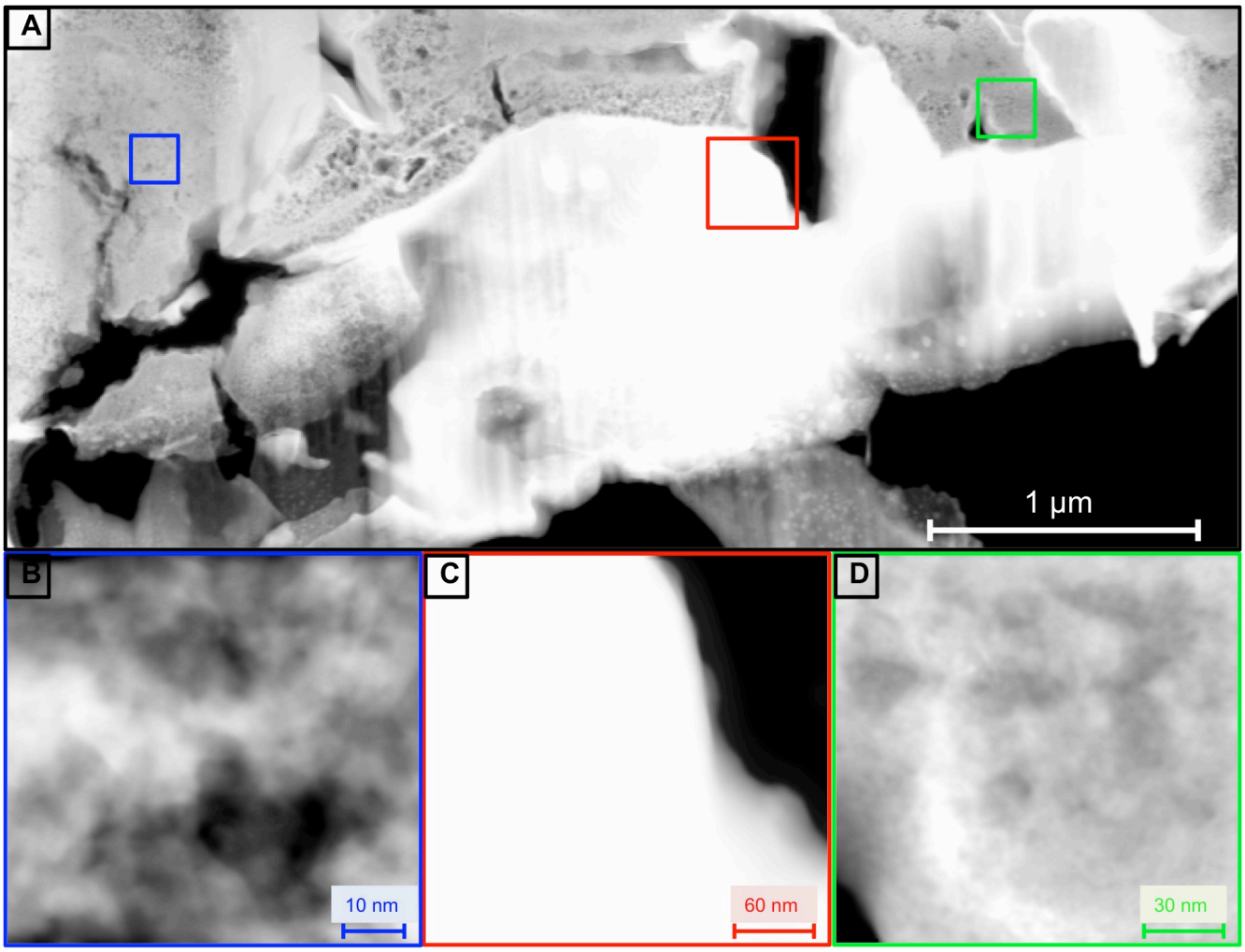

Fig. S1. TEM images of grain from Mundrabilla subsample A. Shown are a larger image (A) and smaller images. Blue (B), red (C) and green (D) colored outlines in larger image correspond to imaged areas (B-D).

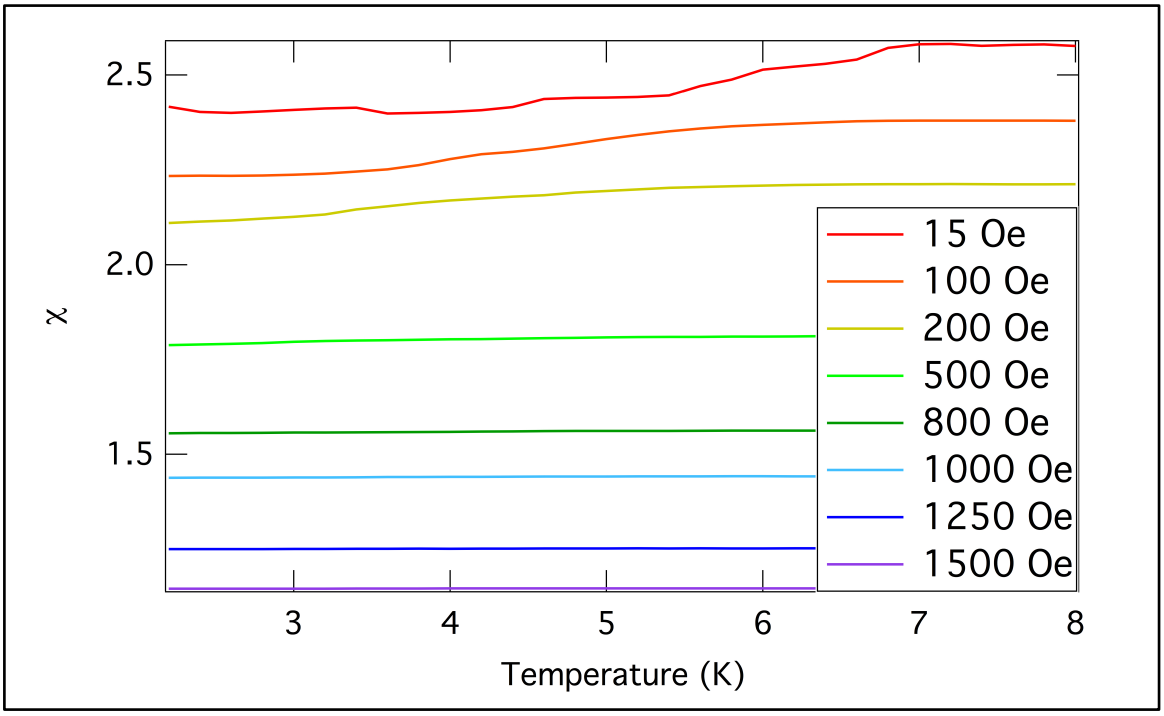

Fig. S2. VSM measurements of samples from Mundrabilla. ZFC measurements on sample MUND-1 were performed with applied magnetic field ranging from 15-1500 Oe. Data is not vertically offset.

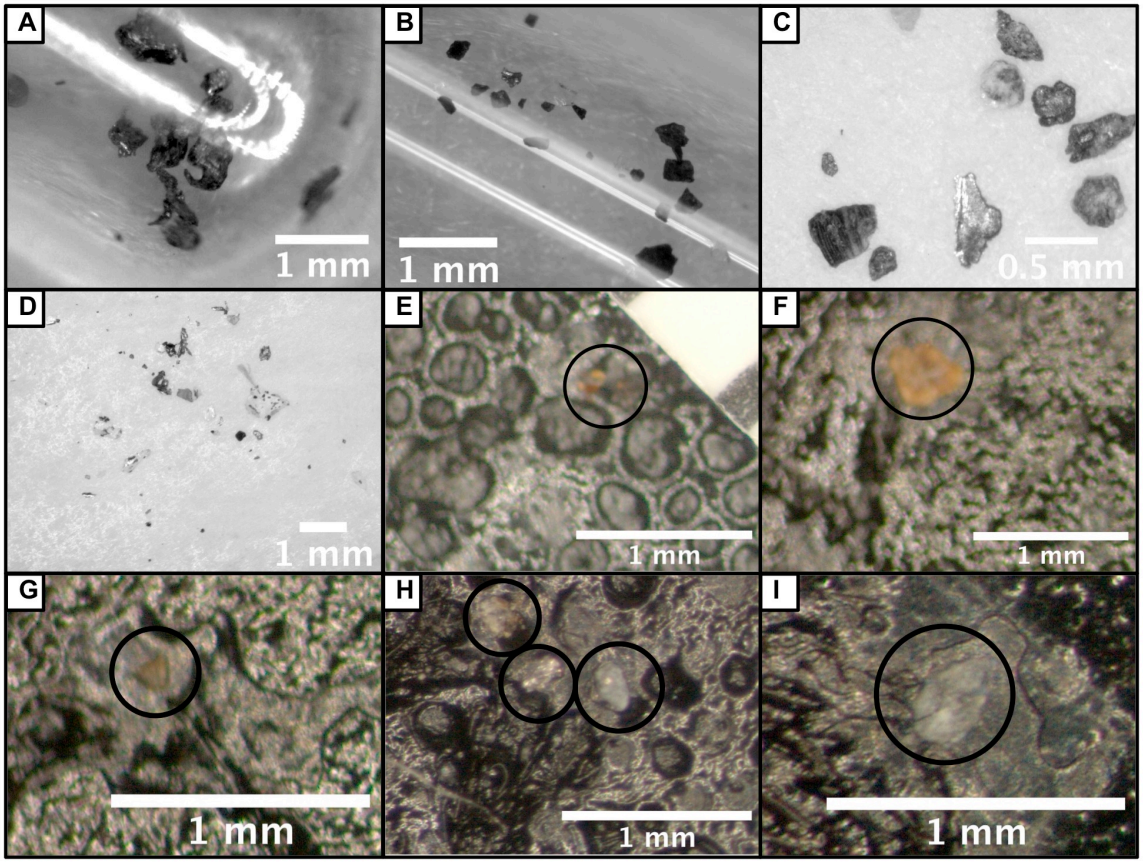

Fig. S3. Images of Meteorite samples and subsamples. Images of MUND-2 subsamples A (a), B (b) and C (c) are shown. Subsamples A and B are imaged inside of quartz tube. Image of MUND-1 (d) is shown. Images of GRA-1 subsamples 1 (e), 2 (f), 3 (g), 4 (h) and 5 (i) are shown on a carbon tape background.

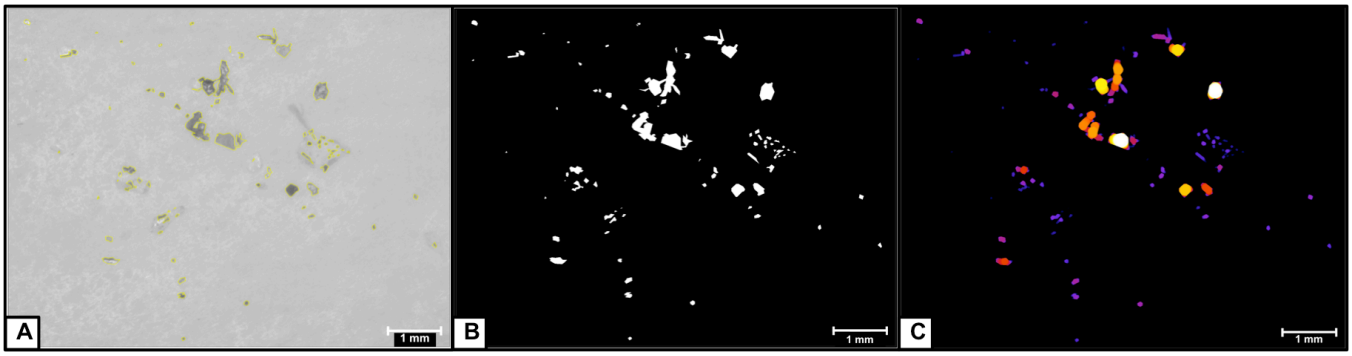

Fig. S4. Method: segmentation and calculation of local thickness. Images produced in ImageJ software for calculation of local thickness. Sample MUND-1 imaged with an optical microscope and outlined in yellow using ImageJ software (a). Mask created of previous image (b). Local thickness calculation based on mask (c) with bright areas indicating large local thickness and dim areas indicating small local thickness.

Table S1. SUPERCON database analysis of subsamples. Cells show maximum volume percentage of a given superconducting phase that could be contained within a given subsample, assuming the EDX measurement of the subsample surface is representative of the whole. Each entry in SUPERCON is separately compared to the EDX measurements. This list is sorted by volume percentage and is a complete analysis of every entry in SUPERCON with a Tc between 5 K and 8 K. Some entries have been condensed into a single entry on this list, (ie: $In_{0.6}Pb_{0.4}$ and $In_{0.5}Pb_{0.5}$ are both listed as In_xPb_y) and the volume for these combined entries is that of the highest individual entry. Entries in the database that are superconducting only under pressure were excluded from the list.

Meteorite	**Mundrabilla**			**GRA 95205**
Subsample	**A**	**B**	**C**	**1**
1st vol. %	In_xPb_y – 38.31%	$Ca_xAl_ySi_z$ – 0.4572%	Pb_xSn_y – 33.89%	MgC_yNi_3 – 2.629%
2nd vol. %	Pb_xSn_y – 35.04%		Pb – 13.70%	$MgC_yNi_{3-z}Fe_z$ – 2.543%
3rd vol. %	In_xSn_y – 25.49%		$Pb_{0.9}Zn_{0.1}$ – 11.92%	In_xSn_y – 1.724%
4th vol. %	$Pb_{0.9}Zn_{0.1}$ – 25.32%			$Ca_xAl_ySi_z$ – 1.033%
5th vol. %	Pb – 24.47%			$Mg_xAl_ySi_z$ – 0.9503%
6th vol. %	Mg_xPb_y – 2.176%			
7th vol. %	$Mg_xAl_ySi_z$ – 0.09144%			
Meteorite	**GRA 95205**			
Subsample	**2**	**3**	**4**	**5**
1st vol. %	C_2Na – 23.90%	$MgCNi_{3-z}Fe_z$ – 1.841%	In_xSn_y – 22.95%	In_xPb_y – 7.324%
2nd vol. %	$Ca_xAl_ySi_z$ – 5.296%	MgC_yNi_3 – 1.720%	In_xPb_y – 20.73%	$Ca_xAl_ySi_z$ – 2.465%
3rd vol. %	NaAlSi – 3.906%		Pb_xSn_y – 10.84%	CaPb – 2.111%
4th vol. %	$Mg_xAl_ySi_z$ – 1.316%		Cu_xSn_y – 6.842%	$Cu_{0.1}Pb_{0.9}$ – 1.829%
5th vol. %			Mg_xPb_y – 6.182%	Mg_xPb_y – 1.792%
6th vol. %			$Cu_{0.1}Pb_{0.9}$ – 5.178%	Pb – 1.769%
7th vol. %			Pb – 5.007%	
8th vol. %			$Mg_xAl_ySi_z$ – 4.597%	
9th vol. %			$MgC_yNi_{3-z}Fe_z$ – 0.9131%	
10th vol. %			$Mg_xC_yNi_3$ – 0.8719%	
11th vol. %			$MgC_yNi_{3-z}Cu_z$ – 0.8523%	

Table S2. TEM EDX measurements of superconducting Mundrabilla Sample. Weight percentage and atomic percentage breakdown of elements from TEM EDX measurements of different sections of a grain from a superconducting sample of Mundrabilla. TEM image of the respective sections is shown in Fig. S1. Errors presented are 1 sigma.

Element	Fig. S1b		Fig. S1c		Fig. S1d	
	Weight %	Atomic %	Weight %	Atomic %	Weight %	Atomic %
In	74.72±10.03	75.32±10.11	76.13±10.15	78.73±10.50	76.85±10.95	67.88±9.67
Sn	15.36±3.58	14.98±3.49	11.21±2.97	11.21±2.97	12.37±3.55	10.56±3.03
Pb	8.75±3.24	4.89±1.81	11.89±3.80	6.81±2.18	5.79±2.98	2.83±1.45
Mg					0.46±0.35	1.91±1.45
Si	1.17±0.50	4.81±2.06	0.77±0.41	3.25±1.73	1.54±0.65	5.57±2.36
Al					2.99±0.89	11.24±3.36
Total	100.00	100.00	100.00	100.00	100.00	99.99

Table S3. List of Meteorites measured with MFMMS. A “yes” in the third column indicates that one or more samples scraped from the meteorite was superconducting.

Meteorite Name	Type	Superconducting
Mundrabilla	Iron IAB	**Yes**
GRA 95205	Ureilite	**Yes**
ALHA77216.85	Ordinary Chondrite (L)	No
LAP 91900	Diogenite	No
Abee	Enstatite Chondrite	No
PCA 82502	Eucrite	No
EET 97511	Ureilite	No
Norton County	Aubrite	No
PCA 91241	Rumuruti Chondrite R3.8-6	No
ALH 81021	Enstatite Chondrite EL6	No
EET 83213	Ordinary Chondrite LL3.7	No
Santa Clara	Iron IVB	No
Allende	Carbonaceous Chondrite CV3	No
LEW 85311	CM Carbonaceous Chondrite (Anomalous)	No
Murchison	Carbonaceous Chondrite CM2	No

Table S4. Volume estimate of Mundrabilla samples and subsamples. ETMUND-2 is the sum of subsamples A, B and C and volume was calculated by added together the preceding subsamples.

	Volume (cm^3)	Error (cm^3)	Area (cm^2)	Local Thickness (cm)	Local Thickness Error (cm)
ETMUND-1	9.10E-5	7.99E-5	9.80E-3	9.29E-3	5.35E-3
ETMUND-2	8.06E-4	5.40E-4			
Subsample A	5.11E-4	3.51E-4	1.58E-2	3.24E-2	1.25E-2
Subsample B	9.37E-5	6.88E-5	5.28E-3	1.77E-2	7.54E-3
Subsample C	2.01E-4	1.20E-4	7.91E-3	2.54E-2	7.45E-3

Table S5. EDX measurements of Mundrabilla subsamples. Weight percentage and atomic percentage breakdown of elements from EDX measurements of Mundrabilla subsamples. Errors presented are 1 sigma.

Element	Subsample A		Subsample B		Subsample C	
	Weight %	Atomic %	Weight %	Atomic %	Weight %	Atomic %
O	38.721±0.171	82.171±0.363	44.501±0.125	73.065±0.206	43.401±0.248	80.070±0.458
Mg	0.028±0.033	0.039±0.045				
Al	0.557±0.052	0.701±0.066	0.202±0.014	0.196±0.014	0.509±0.051	0.557±0.056
Si	1.500±0.045	1.815±0.055	0.168±0.007	0.157±0.007	3.103±0.050	3.262±0.052
P			0.179±0.016	0.152±0.013		
S			1.481±0.017	1.214±0.014		
Cl			0.075±0.007	0.056±0.005	0.319±0.028	0.265±0.024
K			0.061±0.006	0.041±0.004	7.875±0.096	5.945±0.073
Ca			0.156±0.014	0.102±0.009		
Cr			0.303±0.017	0.153±0.008		
Fe	0.490±0.041	0.298±0.025	52.620±0.105	24.751±0.050	0.482±0.044	0.255±0.023
Ni			0.254±0.040	0.113±0.018		
Zn	3.890±0.163	2.022±0.085			0.404±0.075	0.182±0.034
In	17.390±0.300	5.147±0.089				
Sn	12.957±0.345	3.710±0.099			30.205±0.167	7.512±0.042
Pb	24.466±0.985	4.013±0.162			13.701±1.014	1.952±0.145
Total	99.999	100.000	100.000	100.000	99.999	100.000

Table S6. EDX measurements of GRA 95205 subsamples. Weight percentage and atomic percentage breakdown of elements from EDX measurements of GRA 95205 subsamples. Errors presented are 1 standard deviation.

Element	Subsample 1		Subsample 2		Subsample 3	
	Weight %	Atomic %	Weight %	Atomic %	Weight %	Atomic %
O	36.955±0.105	66.517±0.188	61.031±0.236	74.839±0.290	41.112±0.117	55.459±0.158
F					10.861±0.061	12.338±0.070
Na			11.689±0.093	9.976±0.080		
Mg	0.291±0.018	0.345±0.021	0.403±0.035	0.326±0.028	13.911±0.054	12.353±0.048
Al	0.537±0.018	0.573±0.019	1.350±0.053	0.982±0.039		
Si	1.093±0.015	1.121±0.016	2.414±0.047	1.687±0.033	16.613±0.037	12.767±0.029
P	0.094±0.007	0.088±0.007	0.619±0.022	0.392±0.014		
S	1.676±0.014	1.506±0.013	0.957±0.045	0.586±0.028	0.582±0.014	0.392±0.009
Cl	0.074±0.006	0.060±0.005	11.995±0.068	6.638±0.038	0.080±0.007	0.049±0.004
K			4.698±0.060	2.357±0.030		
Ca	0.302±0.008	0.217±0.006	3.681±0.064	1.802±0.031	0.952±0.015	0.513±0.008
Ti			0.145±0.028	0.059±0.011		
Cr	0.144±0.009	0.080±0.005			0.484±0.020	0.201±0.008
Mn					0.181±0.028	0.071±0.011
Fe	51.578±0.096	26.597±0.050	1.016±0.086	0.357±0.030	13.845±0.051	5.351±0.020
Ni	4.226±0.048	2.073±0.023			1.379±0.039	0.507±0.014
Cu						
Zn	0.346±0.027	0.152±0.012				
In	2.471±0.058	0.620±0.014				
Sn	0.213±0.029	0.052±0.007				
I						
Pb						
Total	100.000	100.000	99.998	100.000	100.000	100.000

Element	Subsample 4		Subsample 5	
	Weight %	Atomic %	Weight %	Atomic %
O	55.134±0.158	82.494±0.236	57.412±0.235	88.710±0.363
F				
Na				
Mg	4.801±0.028	4.729±0.027	0.157±0.020	0.159±0.021
Al	0.595±0.026	0.528±0.023	0.699±0.032	0.640±0.029
Si	5.084±0.021	4.334±0.018	0.764±0.027	0.672±0.024
P				
S			0.240±0.016	0.185±0.012
Cl	0.181±0.022	0.122±0.015	0.214±0.015	0.149±0.010
K				
Ca			1.932±0.062	1.192±0.039
Ti				
Cr	0.151±0.012	0.069±0.006		
Mn	0.072±0.016	0.032±0.007		
Fe	3.592±0.040	1.540±0.017	0.371±0.029	0.164±0.013
Ni	0.684±0.044	0.279±0.018		
Cu	0.396±0.051	0.149±0.019	0.621±0.084	0.242±0.033
Zn	0.779±0.064	0.285±0.023		
In	17.065±0.119	3.558±0.025	33.993±0.165	7.319±0.040
Sn	6.458±0.135	1.303±0.027		
I			1.828±0.207	0.356±0.040
Pb	5.007±0.218	0.578±0.025	1.769±0.330	0.211±0.039
Total	100.000	100.000	100.000	100.000